Available online at www.sciencedirect.com
SCIENCE DIRECT®
Comput. Methods Appl. Mech. Engrg. 192 (2003) 3179–3194
Computer methods in applied mechanics and engineering
www.elsevier.com/locate/cma

Constrained inverse formulations in random material design

T.I. Zohdi *

Department of Mechanical Engineering, University of California, 6195 Etcheverry Hall, Berkeley, CA 94720-1740, USA

Received 12 May 2003; accepted 12 May 2003

Abstract

The focus of this work is on the development of a computational strategy to design materials composed of randomly dispersed particulates suspended in a homogeneous binding matrix. The design objectives are to deliver prescribed macroscopic effective responses while simultaneously obeying constraints that reflect the distortion of the microscale stress fields, as well as the likelihood for fatigue damage. A nonderivative statistical genetic algorithm is developed which can handle difficulties in designing materials with random particulate microstructure due to objective function nonconvexity and lack of objective function regularity. Theoretical aspects are investigated and three-dimensional numerical examples are given.

Keywords: Random materials; Genetic algorithms; Exterior point methods; Fatigue-resistance

1. Computational material design

In this work, we are primarily concerned with the construction and solution of inverse problems describing the design of materials composed of randomly dispersed particulates suspended in a homogeneous binding matrix. The design objectives are to find sets of microstructural parameters, such as the relative volume fractions of the constituents, the geometries of the particulates and their mechanical properties, which minimize

$$\Pi = \left(\frac{\| \mathbb{E}^* - \mathbb{E}^{*,\mathrm{D}} \|}{\| \mathbb{E}^{*,\mathrm{D}} \|} \right)^{q_0}, \tag{1.1}$$

where $0 < q_0 < \infty$, while simultaneously obeying constraints on the microscale stress field behavior. The constraints will be specified shortly. Here $\mathbb{E}^{*,\mathrm{D}}$ is a prespecified desired effective response, $\mathbb{E}^*$ is the effective response described via $\langle \boldsymbol{\sigma} \rangle_\Omega = \mathbb{E}^* : \langle \boldsymbol{\epsilon} \rangle_\Omega$, where $\langle \cdot \rangle_\Omega \stackrel{\text{def}}{=} \frac{1}{|\Omega|} \int_\Omega \mathrm{d}\Omega$, and where $\boldsymbol{\sigma}$ and $\boldsymbol{\epsilon}$ are the stress and strain

* Tel.: +1-510-642-6834; fax: +1-510-642-6163.
E-mail address: zohdi@newton.berkeley.edu (T.I. Zohdi).

0045-7825/03/$ - see front matter
doi:10.1016/S0045-7825(03)00345-1

tensor fields within a statistically representative volume element of volume $|\Omega|$, produced by a trial microstructure. [1] If the effective response is assumed isotropic, which is the case if the particles are randomly distributed and randomly oriented (if nonspherical), then the effective bulk and shear moduli are given by

$$3\kappa^* \stackrel{\text{def}}{=} \frac{\langle \text{tr}\boldsymbol{\sigma}/3\rangle_\Omega}{\langle \text{tr}\boldsymbol{\epsilon}/3\rangle_\Omega} \quad \text{and} \quad 2\mu^* \stackrel{\text{def}}{=} \sqrt{\frac{\langle \boldsymbol{\sigma}'\rangle_\Omega : \langle \boldsymbol{\sigma}'\rangle_\Omega}{\langle \boldsymbol{\epsilon}'\rangle_\Omega : \langle \boldsymbol{\epsilon}'\rangle_\Omega}}.$$

An extensive review of the state of the art in the analysis of random heterogeneous media can be found in the work of Torquato [58–62].

In order to systematize the computational minimization process, we characterize a microstructural design through an N-tuple design vector, denoted $\boldsymbol{\Lambda} \stackrel{\text{def}}{=} (\Lambda_1, \Lambda_2, \ldots, \Lambda_N)$, representing the following components. (I) *Particulate mechanical properties:* for example, assuming local isotropy of the particles, the bulk and shear moduli, κ_2 and μ_2 (two variables), (II) *particulate topology:* where we characterize the shape of the particulates by a generalized ellipsoidal equation:

$$\left(\frac{|x-x_0|}{r_1}\right)^{s_1} + \left(\frac{|y-y_0|}{r_2}\right)^{s_2} + \left(\frac{|z-z_0|}{r_3}\right)^{s_3} = 1, \tag{1.2}$$

where the s's are exponents. Values of $s < 1$ produce nonconvex shapes, while $s > 2$ values produce "block-like" shapes (three design variables), (III) *particulate aspect ratio:* for example, defined by $\text{AR} \stackrel{\text{def}}{=} \frac{r_1}{r_2} = \frac{r_1}{r_3}$, where $r_2 = r_3$, $\text{AR} > 1$ for prolate geometries and $\text{AR} < 1$ for oblate shapes (one variable) and (IV) *particulate volume fraction:* for example, $v_2 \stackrel{\text{def}}{=} \frac{|\Lambda|}{|\Omega|}$, where $|\Lambda|$ is the volume occupied by the particles, and $|\Omega|$ is the total volume of the material (one variable). Therefore we have a total of seven design variables, $\boldsymbol{\Lambda} = (\kappa_2, \mu_2, \text{AR}, v_2, s_1, s_2, s_3)$. Although we will not consider the matrix material's properties as being free variables, this poses no additional difficulties.

2. Characteristic of such objectives

Some key difficulties encountered in such problems, which we now discuss, are (1) nonconvexity of objective functions such as in Eq. (1.1), due to the variety of design variables, (2) objective functions which are not continuously differentiable because of active–inactive constraints and (3) sample size effects, which induce a degree of stochastic behavior into the objective function.

2.1. Nonconvexity

Consider a one-dimensional heterogeneous bar composed of two materials, E_1 and E_2 (transverse bonded strips), each occupying volume fractions v_1 and v_2 ($v_1 + v_2 = 1$), respectively. The effective mechanical response for such a system, $\mathbb{E}^*$, $\langle \boldsymbol{\sigma}\rangle_\Omega \stackrel{\text{def}}{=} E^* \langle \boldsymbol{\epsilon}\rangle_\Omega$, is the harmonic average, which can be written as $E^* = \frac{\tau E_1}{(1-v_2)\tau + v_2}$, where $\tau = \frac{E_2}{E_1}$, Clearly, there is no unique combination of τ and v_2 to produce the same desired effective response. Consider the objective, $\Pi = \left(\frac{E^* - E^{*,\text{D}}}{E^{*,\text{D}}}\right)^2$, where $E^{*,\text{D}}$ is the desired effective response. If one were to pursue a standard Newton-type multivariate search for a new design increment one would construct the following Hessian system for the two design variables, $\boldsymbol{\Lambda} = (\tau, v_2)$:

[1] At the microscale, the mechanical properties of microheterogeneous materials are characterized by a spatially variable elasticity tensor $\mathbb{E}$. The symbol $\|\cdot\|$ is an appropriate admissible norm to be discussed later.

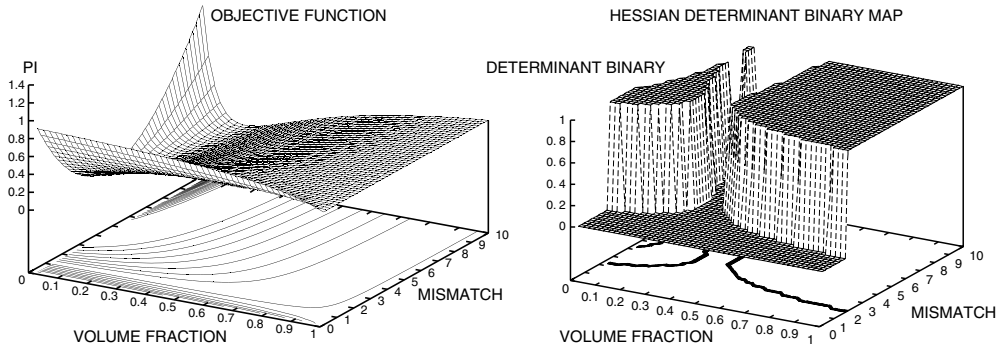

Fig. 1. Left: The behavior of the objective function for $E_1 = 1$ and $E^{*,D} = 4$. Right: A binary map of the behavior of the determinant of the Hessian of the objective function for $E_1 = 1$ and $E^{*,D} = 4$. Here a value of 1 indicates a positive definite Hessian and 0 indicates a nonpositive Hessian.

$$\begin{bmatrix} \dfrac{\partial^2 \Pi(\tau, v_2)}{\partial \tau^2} & \dfrac{\partial^2 \Pi(\tau, v_2)}{\partial \tau \, \partial v_2} \\ \dfrac{\partial^2 \Pi(\tau, v_2)}{\partial v_2 \, \partial \tau} & \dfrac{\partial^2 \Pi(\tau, v_2)}{\partial v_2^2} \end{bmatrix} \begin{Bmatrix} \Delta\tau \\ \Delta v_2 \end{Bmatrix} = - \begin{Bmatrix} \dfrac{\partial \Pi(\tau, v_2)}{\partial \tau} \\ \dfrac{\partial \Pi(\tau, v_2)}{\partial v_2} \end{Bmatrix}. \tag{2.1}$$

Unfortunately, this system becomes noninvertible throughout the design space, due to the nonconvexity of the objective function Π, as illustrated in Fig. 1. The behavior of such objectives becomes even worse when more design variables are present, such as in three-dimensional cases involving topological variables discussed earlier. For more detailed discussions of such issues see Cherkaev [5].

2.2. Size effects

We remark that even if the issues of nonconvexity and nondifferentiability of the objective were not present, and one were to attempt to apply a gradient-type approach, the construction of numerical derivatives of the objective function can become highly unstable. This is due to the fact that effective responses of finite sized samples, of equal volume but of different random particle distributions, exhibit mutual fluctuations, leading to amplified noise in optimization strategies where objective function sensitivities (derivatives) are needed (Fig. 2). For example, referring to Fig. 2, the effects of fluctuations due to sample size can be characterized by computing the difference between the smallest value on the right of an arbitrary design point $\mathbf{\Lambda}^0$, due to size effects, and the largest value on the left, also due to size effects, resulting in

$$\delta^- = \Pi^-(\mathbf{\Lambda}^0 + \Delta\mathbf{\Lambda}) - \Pi^+(\mathbf{\Lambda}^0 - \Delta\mathbf{\Lambda}) \tag{2.2}$$

and computing the difference between the largest value on the right and smallest value on the left, resulting in

$$\delta^+ = \Pi^+(\mathbf{\Lambda}^0 + \Delta\mathbf{\Lambda}) - \Pi^-(\mathbf{\Lambda}^0 - \Delta\mathbf{\Lambda}). \tag{2.3}$$

Denoting the uncertainty in the objective function's value at $\mathbf{\Lambda}^0 + \Delta\mathbf{\Lambda}$ by $\mathscr{U}(\mathbf{\Lambda}^0 + \Delta\mathbf{\Lambda}) \stackrel{\text{def}}{=} \Pi^+(\mathbf{\Lambda}^0 + \Delta\mathbf{\Lambda}) - \Pi^-(\mathbf{\Lambda}^0 + \Delta\mathbf{\Lambda})$ and the uncertainty in the objective function's value at $\mathbf{\Lambda}^0 - \Delta\mathbf{\Lambda}$ by $\mathscr{U}(\mathbf{\Lambda}^0 - \Delta\mathbf{\Lambda}) \stackrel{\text{def}}{=} \Pi^+(\mathbf{\Lambda}^0 - \Delta\mathbf{\Lambda}) - \Pi^-(\mathbf{\Lambda}^0 - \Delta\mathbf{\Lambda})$, we have an uncertainty in the sensitivity

$$0 \leqslant |\delta^+ - \delta^-| = \mathscr{U}(\mathbf{\Lambda}^0 + \Delta\mathbf{\Lambda}) + \mathscr{U}(\mathbf{\Lambda}^0 - \Delta\mathbf{\Lambda}). \tag{2.4}$$

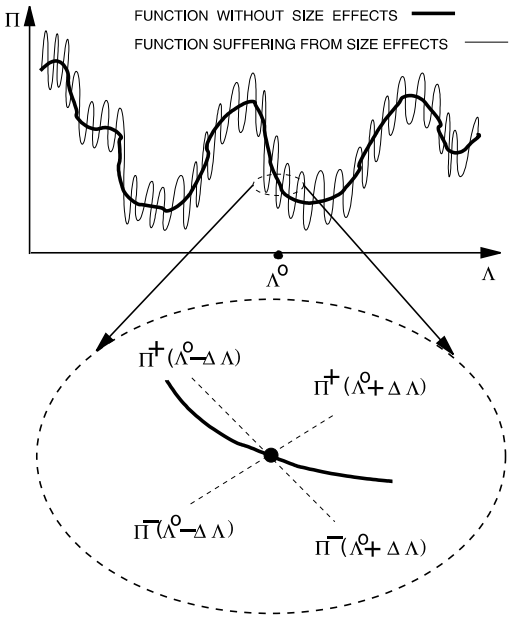

Fig. 2. An objective function suffering from size effects.

Clearly, the effects of the fluctuations are amplified for the sensitivities. Therefore, even for large samples of randomly dispersed particulate material, which may exhibit slight fluctuations from one another, the resulting deviations in derivatives can be quite large. For further details see [68,72]. Furthermore, when active–inactive constraints are introduced, as they later will be, the objective function will become not continuously differentiable throughout the domain, in locations that are indeterminant a priori. In summary, for the class of problems considered here, gradient methods should be avoided due to (I) nonconvexity leading to uninvertible Hessians and (II) noise in the numerical derivatives of the objective function. In addition, a further issue arises, namely nondifferentiability of the constraints, in particular active–inactive constraints, as well as, in some cases, nondifferentiability of the unconstrained objective function itself. This further motivates, later in the analysis, a nonderivative (genetic) search procedure.

3. Introduction of constraints

A drawback of adding particulate material to a homogeneous base matrix is that the presence of second phase particles will perturb the otherwise smooth stress fields in the matrix, locally amplifying or reducing the fields throughout the microstructure. Thus, it makes sense to account for this distortion and to attempt to limit it during the design process.

Consider the deviation of the stress field from its volumetric average, $\delta\boldsymbol{\sigma} = \boldsymbol{\sigma} - \langle\boldsymbol{\sigma}\rangle_{\Omega}$, measured in the following norm ($q > 0$):

$$\|\delta\boldsymbol{\sigma}\|^{q}_{L^{q}(\Omega)} \stackrel{\text{def}}{=} \frac{1}{|\Omega|}\int_{\Omega}(\delta\boldsymbol{\sigma} : \delta\boldsymbol{\sigma})^{q}\,\mathrm{d}\Omega \geqslant 0. \tag{3.1}$$

The physical meaning of this norm, for $q = 1$, is the standard deviation of the stress field from its volumetric average. Higher q indicate more sensitive measures to the differences between the internal field and its average. A meaningful constraint is

$$w_q P_q(\boldsymbol{\Lambda}) = w_q \,\mathrm{Max}\left(0, \left(\frac{\|\delta\boldsymbol{\sigma}\|^q_{L^q(\Omega)}}{\mathrm{TOL}_q \|\boldsymbol{\sigma}\|^q_{L^q(\Omega)}} - 1\right)\right). \tag{3.2}$$

To add an entire range of "higher stress moment" constraints, we write

$$\boldsymbol{w}\mathbb{P}(\boldsymbol{\Lambda}) \stackrel{\mathrm{def}}{=} \sum_{q=1}^{N} w_q P_q(\boldsymbol{\Lambda}), \tag{3.3}$$

where the components of $\boldsymbol{q} = (q_1, q_2, \ldots, q_N)$ and $\boldsymbol{w} = (w_1, w_2, \ldots, w_N)$ are nonnegative. The final augmented function is

$$\Pi^P(\boldsymbol{\Lambda}, \boldsymbol{w}) = \underbrace{\left(\frac{\|\mathbb{E}^* - \mathbb{E}^{*,\mathrm{D}}\|}{\|\mathbb{E}^{*,\mathrm{D}}\|}\right)^{q_0}}_{\text{Macromoduli}} + \underbrace{\boldsymbol{w}\mathbb{P}(\boldsymbol{\Lambda})}_{\text{Microfield distortion}} . \tag{3.4}$$

For an isotropic objective we write

$$\Pi^P = w_\kappa \underbrace{\left(\frac{\kappa^* - \kappa^{*,\mathrm{D}}}{\kappa^{*,\mathrm{D}}}\right)^{q_0}}_{\text{Macroscopic bulk}} + w_\mu \underbrace{\left(\frac{\mu^* - \mu^{*,\mathrm{D}}}{\mu^{*,\mathrm{D}}}\right)^{q_0}}_{\text{Macroscopic shear}} + \underbrace{\sum_{q=1}^{N} w_q P_q(\Lambda)}_{\text{Microfield distortion}} . \tag{3.5}$$

Essentially this is an exterior point (penalty) method to enforce constraints. Let us define the following penalized function $\Pi^P(\boldsymbol{\Lambda}_K, \boldsymbol{w}^K) \stackrel{\mathrm{def}}{=} \Pi(\boldsymbol{\Lambda}_K) + \boldsymbol{w}^K\mathbb{P}(\boldsymbol{\Lambda}_K)$, where (1) $\mathbb{P}(\boldsymbol{\Lambda}_K) \in C^0(\mathbb{R}^N)$, (2) $\mathbb{P}(\boldsymbol{\Lambda}_K) \geqslant 0$ and (3) $\mathbb{P}(\boldsymbol{\Lambda}_K) = 0$, if and only if $\boldsymbol{\Lambda}_K \in \Theta_{\mathrm{f}}$, $\Theta_{\mathrm{f}} \stackrel{\mathrm{def}}{=}$ the feasible region. We have the following properties, where $\boldsymbol{\Lambda}^*_K$ is the minimizer of Π^P for weight $\boldsymbol{w}^K$ and $\boldsymbol{\Lambda}^*$ is a true minimizer Π with the constraints:

$$\boxed{\begin{array}{l}
\text{(a) } \Pi^P(\boldsymbol{\Lambda}^*_K, \boldsymbol{w}^K) \leqslant \Pi^P(\boldsymbol{\Lambda}^*_{K+1}, \boldsymbol{w}^{K+1}),\\
\text{(b) } \mathbb{P}(\boldsymbol{\Lambda}^*_{K+1}) \leqslant \mathbb{P}(\boldsymbol{\Lambda}^*_K),\\
\text{(c) } \Pi(\boldsymbol{\Lambda}^*_K) \leqslant \Pi(\boldsymbol{\Lambda}^*_{K+1}),\\
\text{(d) } \Pi(\boldsymbol{\Lambda}^*_K) \leqslant \Pi^P(\boldsymbol{\Lambda}^*_K, \boldsymbol{w}^K) \leqslant \Pi(\boldsymbol{\Lambda}^*),\\
\text{(e) } \lim\limits_{\boldsymbol{w}^K \to \infty} \Pi^P(\boldsymbol{\Lambda}^*_K, \boldsymbol{w}^K) = \Pi(\boldsymbol{\Lambda}^*).
\end{array}} \tag{3.6}$$

The proofs are constructive and follow. By definition

$$\begin{aligned}
\Pi^P(\boldsymbol{\Lambda}^*_{K+1}, \boldsymbol{w}^{K+1}) &= \Pi(\boldsymbol{\Lambda}^*_{K+1}) + \boldsymbol{w}^{K+1}\mathbb{P}(\boldsymbol{\Lambda}^*_{K+1})\\
&\geqslant \Pi(\boldsymbol{\Lambda}^*_{K+1}) + \boldsymbol{w}^{K}\mathbb{P}(\boldsymbol{\Lambda}^*_{K+1})\\
&\geqslant \Pi(\boldsymbol{\Lambda}^*_{K}) + \boldsymbol{w}^{K}\mathbb{P}(\boldsymbol{\Lambda}^*_{K}) \stackrel{\mathrm{def}}{=} \Pi^P(\boldsymbol{\Lambda}^*_K, \boldsymbol{w}^K) \Rightarrow \text{(a)}.
\end{aligned} \tag{3.7}$$

By definition

$$\Pi(\boldsymbol{\Lambda}^*_K) + \boldsymbol{w}^K\mathbb{P}(\boldsymbol{\Lambda}^*_K) \leqslant \Pi(\boldsymbol{\Lambda}^*_{K+1}) + \boldsymbol{w}^K\mathbb{P}(\boldsymbol{\Lambda}^*_{K+1}) \tag{3.8}$$

and

$$\Pi(\boldsymbol{\Lambda}^*_{K+1}) + \boldsymbol{w}^{K+1}\mathbb{P}(\boldsymbol{\Lambda}^*_{K+1}) \leqslant \Pi(\boldsymbol{\Lambda}^*_K) + \boldsymbol{w}^{K+1}\mathbb{P}(\boldsymbol{\Lambda}^*_K). \tag{3.9}$$

Adding the two previous results yields

$$(\boldsymbol{w}^{K+1} - \boldsymbol{w}^{K})\mathbb{P}(\boldsymbol{\Lambda}^{*}_{K+1}) \leqslant (\boldsymbol{w}^{K+1} - \boldsymbol{w}^{K})\mathbb{P}(\boldsymbol{\Lambda}^{*}_{K}) \Rightarrow \text{(b)}. \tag{3.10}$$

Since $\boldsymbol{\Lambda}_K$ is a minimizer of the augmented form

$$\Pi(\boldsymbol{\Lambda}^{*}_{K+1}) + \boldsymbol{w}^{K}\mathbb{P}(\boldsymbol{\Lambda}^{*}_{K+1}) \geqslant \Pi(\boldsymbol{\Lambda}^{*}_{K}) + \boldsymbol{w}^{K}\mathbb{P}(\boldsymbol{\Lambda}^{*}_{K}). \tag{3.11}$$

From part (b) we have $\mathbb{P}(\boldsymbol{\Lambda}^{*}_{K+1}) \leqslant \mathbb{P}(\boldsymbol{\Lambda}^{*}_{K})$, which, when combined with the above yields

$$\Pi(\boldsymbol{\Lambda}^{*}_{K+1}) + \boldsymbol{w}^{K}\mathbb{P}(\boldsymbol{\Lambda}^{*}_{K}) \geqslant \Pi(\boldsymbol{\Lambda}^{*}_{K+1}) + \boldsymbol{w}^{K}\mathbb{P}(\boldsymbol{\Lambda}^{*}_{K+1}) \geqslant \Pi(\boldsymbol{\Lambda}^{*}_{K}) + \boldsymbol{w}^{K}\mathbb{P}(\boldsymbol{\Lambda}^{*}_{K}) \Rightarrow \text{(c)}. \tag{3.12}$$

For each K,

$$\Pi(\boldsymbol{\Lambda}^{*}) \stackrel{\text{def}}{=} \Pi(\boldsymbol{\Lambda}^{*}) + \underbrace{\boldsymbol{w}^{K}\mathbb{P}(\boldsymbol{\Lambda}^{*})}_{=0} \geqslant \Pi(\boldsymbol{\Lambda}^{*}_{K}) + \boldsymbol{w}^{K}\mathbb{P}(\boldsymbol{\Lambda}^{*}_{K}) \stackrel{\text{def}}{=} \Pi^{P}(\boldsymbol{\Lambda}^{*}_{K}, \boldsymbol{w}^{K}) \geqslant \Pi(\boldsymbol{\Lambda}^{*}_{K}) \Rightarrow \text{(d)}. \tag{3.13}$$

Utilizing the previous results, one can show that the method converges. Let $\{\boldsymbol{\Lambda}^{*}_{K}\}$, $K \in \mathcal{Q}$, be a convergent subsequence of $\{\boldsymbol{\Lambda}^{*}_{K}\}$, having limit $\hat{\boldsymbol{\Lambda}}$. Therefore, assuming continuity of Π we have $\lim_{K\in\mathcal{Q}} \Pi(\boldsymbol{\Lambda}^{*}_{K}) = \Pi(\hat{\boldsymbol{\Lambda}})$. From the previous results

$$\Pi^{P}(\boldsymbol{\Lambda}^{*}_{K+1}, \boldsymbol{w}^{K+1}) \geqslant \Pi^{P}(\boldsymbol{\Lambda}^{*}_{K}, \boldsymbol{w}^{K}), \tag{3.14}$$

which implies

$$\lim_{K\in\mathcal{Q}} \Pi^{P}(\boldsymbol{\Lambda}^{*}_{K}, \boldsymbol{w}^{K}) \stackrel{\text{def}}{=} \Pi^{P*} \leqslant \Pi(\boldsymbol{\Lambda}^{*}) \quad \text{(By d)}. \tag{3.15}$$

Therefore,

$$\Pi^{P*}(\boldsymbol{\Lambda}^{*}) - \Pi(\hat{\boldsymbol{\Lambda}}) = \lim_{K\in\mathcal{Q}} \boldsymbol{w}^{K}\mathbb{P}(\boldsymbol{\Lambda}^{*}_{K}) \leqslant \infty, \tag{3.16}$$

which implies $\lim_{K\in\mathcal{Q}} \mathbb{P}(\boldsymbol{\Lambda}^{*}_{K}) = 0$. Since $\mathbb{P}(\boldsymbol{\Lambda}^{*}_{K})$ is continuous, $\mathbb{P}(\hat{\boldsymbol{\Lambda}}) = 0$, and therefore $\hat{\boldsymbol{\Lambda}}$ is feasible. $\hat{\boldsymbol{\Lambda}}$ must be optimal since, $\boldsymbol{\Lambda}^{*}_{K} \to \hat{\boldsymbol{\Lambda}}$ and

$$\Pi(\hat{\boldsymbol{\Lambda}}) = \lim_{K\in\mathcal{Q}} \Pi(\boldsymbol{\Lambda}^{*}_{K}) \leqslant \Pi(\boldsymbol{\Lambda}^{*}) \Rightarrow \text{(e)}. \tag{3.17}$$

Remarks: By increasing the penalty weights, we force the augmented form's sequence to approach the unaugmented optimum from below. For general properties of exterior point methods see [7] or [45].

4. Related fatigue constraints for microheterogeneous solids

As mentioned during the construction of the distortion constraints, a drawback of adding particulate material to a homogeneous base matrix is that the presence of a second phase particles will perturb the otherwise smooth stress fields in the matrix. This locally amplifies the stress field intensity throughout the microstructure. Under cyclic loading, this can lead to fatigue-induced damage. Therefore, when designing new solids with heterogeneous microstructure, estimates of the aggregate amount of fatigue damage are valuable in characterizing the long term performance of the material. Accordingly, we construct constraints, representing tolerable damage limits, in a similar way as for the distortion measures.

4.1. Classical fatigue relations

At a material point, the classical Basquin relation for fatigue life estimation are as follows [1]:

$$\|\boldsymbol{\sigma}_a\| = (\|\boldsymbol{\sigma}_{\mathrm{f}}\| - \|\boldsymbol{\sigma}_{\mathrm{m}}\|)(2N_{\mathrm{f}})^b \Rightarrow N_{\mathrm{f}} = \frac{1}{2}\left(\frac{\|\boldsymbol{\sigma}_a\|}{\|\boldsymbol{\sigma}_{\mathrm{f}}\| - \|\boldsymbol{\sigma}_{\mathrm{m}}\|}\right)^{1/b}, \tag{4.1}$$

which has been extended to a multiaxial stress state by use of Euclidean norms ($\|\boldsymbol{\sigma}\| \stackrel{\mathrm{def}}{=} \sqrt{\boldsymbol{\sigma} : \boldsymbol{\sigma}}$). Here the norm of the mean stress is $\|\boldsymbol{\sigma}_{\mathrm{m}}\| = \frac{\|\boldsymbol{\sigma}_{\max} + \boldsymbol{\sigma}_{\min}\|}{2}$ while the norm of the fluctuating stress is $\|\boldsymbol{\sigma}_a\| = \frac{\|\boldsymbol{\sigma}_{\max} - \boldsymbol{\sigma}_{\min}\|}{2}$, where we denote static failure stress by $\boldsymbol{\sigma}_{\mathrm{f}}$ and typically, $-0.12 \leqslant b \leqslant -0.05$. Classical relations of this type, which hold at a material point, are discussed in [57].

4.2. Construction of a constraint

Clearly, from direct numerical computations, say with the finite element method, one can post-process the stresses, by using Eq. (4.1), directly to compute the estimated fatigue life of every point $\boldsymbol{x}_k$, denoted by $N_{\mathrm{f}k}$. Once the $N_{\mathrm{f}k}$'s are computed, we employ classical Palmgren [55]–Miner [47] accumulated damage relations, $\kappa_k^n = \mathrm{Max}\left(0, 1 - \frac{n}{N_{\mathrm{f}k}}\right)\kappa_k^0$ and $\mu_k^n = \mathrm{Max}\left(0, 1 - \frac{n}{N_{\mathrm{f}k}}\right)\mu_k^0$, where κ_k^0 and μ_k^0 are the undamaged values of the bulk and shear moduli at $\boldsymbol{x}_k$, respectively, and n is the number of applied load cycles. In the isotropic case, the damage is simply

$$\alpha_k^n \stackrel{\mathrm{def}}{=} \frac{\kappa_k^n}{\kappa_k^0} = \frac{\mu_k^n}{\mu_k^0} = \mathrm{Max}\left(0, \left(1 - \frac{n}{N_{\mathrm{f}k}}\right)\right). \tag{4.2}$$

The overall fatigue damage is characterized volumetric average, $\langle \alpha^n \rangle_\Omega$. A fatigue constraint is constructed first by setting a tolerance, where ideally,

$$\langle \alpha^n \rangle_\Omega > \mathrm{TOL}_\alpha \tag{4.3}$$

which is then incorporated as an active–inactive unilateral condition into a design cost function, which we intend to minimize ($q_0, q_{\mathrm{F}} > 0$)

$$\Pi^P = \underbrace{\left(\frac{\|\mathbb{E}^* - \mathbb{E}^{*,\mathrm{D}}\|}{\|\mathbb{E}^{*,\mathrm{D}}\|}\right)^{q_0}}_{\text{Macro-objective}} + \underbrace{w_{\mathrm{F}} P_{\mathrm{F}}}_{\text{Fatigue damage}}, \tag{4.4}$$

where

$$w_{\mathrm{F}} P_{\mathrm{F}} \stackrel{\mathrm{def}}{=} w_{\mathrm{F}}\left(\mathrm{Max}\left(0, \left(\frac{\mathrm{TOL}_\alpha - \langle \alpha^n \rangle_\Omega}{\mathrm{TOL}_\alpha}\right)\right)\right)^{q_{\mathrm{F}}}. \tag{4.5}$$

In the isotropic case, we write

$$\Pi^P = w_\kappa\left(\frac{\kappa^* - \kappa^{*,\mathrm{D}}}{\kappa^{*,\mathrm{D}}}\right)^{q_0} + w_\mu\left(\frac{\mu^* - \mu^{*,\mathrm{D}}}{\mu^{*,\mathrm{D}}}\right)^{q_0} + w_{\mathrm{F}} P_{\mathrm{F}}. \tag{4.6}$$

Remark I: As in the case of distortion constraints, the formulation in Eq. (3.5) is an exterior point (penalty) method to enforce constraints. Therefore, by increasing the penalty weight, we force the augmented form approach the unaugmented optimum from below. In other words, as the penalty parameter is increased, the exterior point formulation more accurately approximates the original constrained problem. However, the exterior point formulation becomes harder to minimize with gradient based methods, if they are applicable, due to ill conditioning. However, this appears to be a nonissue for nonderivative methods.

Remark II: One can restrict the constraint activation to specific "zones of interest" by simply adding a weighting function during the computation of the average damage, $\phi(\langle \alpha^n \rangle_\Omega)$, where $\phi = 0$ outside of the

zones. For example, such zones could be interfacial regions enveloping the material interfaces between the matrix and particles.

4.3. Qualitative behavior of the fatigue constraints

One way to qualitatively characterize the aggregate fatigue damage is via concentration tensors, which provide a measure of the deviation away from the mean fields throughout the material. One may write $\langle \boldsymbol{\sigma} \rangle_{\Omega} = \frac{1}{|\Omega|}(\int_{\Omega_1} \boldsymbol{\sigma}\, d\Omega + \int_{\Omega_2} \boldsymbol{\sigma}\, d\Omega) = v_1 \langle \boldsymbol{\sigma} \rangle_{\Omega_1} + v_2 \langle \boldsymbol{\sigma} \rangle_{\Omega_2}$, where Ω_1 is the volume of the matrix phase and Ω_2 is the volume fraction of the second phase, and consequently

$$\langle \boldsymbol{\sigma} \rangle_{\Omega} = v_1 \langle \boldsymbol{\sigma} \rangle_{\Omega_1} + v_2 \langle \boldsymbol{\sigma} \rangle_{\Omega_2} = ((\mathbb{I}_1 + v_2(\mathbb{I}_2 - \mathbb{I}_1)) : \boldsymbol{C}) : \langle \boldsymbol{\epsilon} \rangle_{\Omega}, \tag{4.7}$$

where $\boldsymbol{C} : \langle \boldsymbol{\epsilon} \rangle_{\Omega} = \langle \boldsymbol{\epsilon} \rangle_{\Omega_2}$, $\boldsymbol{C} \stackrel{\text{def}}{=} (\frac{1}{v_2}(\mathbb{I}_2 - \mathbb{I}_1)^{-1} : (\mathbb{I}^* - \mathbb{I}_1))$. Thereafter, we may write, for the variation in the stress, $\boldsymbol{C} : \mathbb{I}^{*-1} : \langle \boldsymbol{\sigma} \rangle_{\Omega} = \mathbb{I}_2^{-1} : \langle \boldsymbol{\sigma} \rangle_{\Omega_2}$, which reduces to $\mathbb{I}_2 : \boldsymbol{C} : \mathbb{I}^{*-1} : \langle \boldsymbol{\sigma} \rangle_{\Omega} \stackrel{\text{def}}{=} \widehat{\boldsymbol{C}} : \langle \boldsymbol{\sigma} \rangle_{\Omega} = \langle \boldsymbol{\sigma} \rangle_{\Omega_2}$, where $\widehat{\boldsymbol{C}}$ is known as the stress concentration tensor. Therefore, once either $\widehat{\boldsymbol{C}}$ or $\mathbb{I}^*$ are known, the other can be determined. Clearly, the microstress fields are minimally distorted when $\widehat{\boldsymbol{C}} = \boldsymbol{I}$. For the matrix, we have

$$\langle \boldsymbol{\sigma} \rangle_{\Omega_1} = \frac{\langle \boldsymbol{\sigma} \rangle_{\Omega} - v_2 \langle \boldsymbol{\sigma} \rangle_{\Omega_2}}{v_1} = \langle \boldsymbol{\sigma} \rangle_{\Omega_1} = \frac{\langle \boldsymbol{\sigma} \rangle_{\Omega} - v_2 \widehat{\boldsymbol{C}} : \langle \boldsymbol{\sigma} \rangle_{\Omega}}{v_1} = \frac{(\boldsymbol{I} - v_2 \widehat{\boldsymbol{C}}) : \langle \boldsymbol{\sigma} \rangle_{\Omega}}{v_1} = \widehat{\widehat{\boldsymbol{C}}} : \langle \boldsymbol{\sigma} \rangle_{\Omega}. \tag{4.8}$$

We have for the alternating stresses, $\langle \boldsymbol{\sigma}_a \rangle_{\Omega_2} = \widehat{\boldsymbol{C}} : \langle \boldsymbol{\sigma}_a \rangle_{\Omega}$ and $\langle \boldsymbol{\sigma}_a \rangle_{\Omega_1} = \widehat{\widehat{\boldsymbol{C}}} : \langle \boldsymbol{\sigma}_a \rangle_{\Omega}$, as well as for the mean stresses $\langle \boldsymbol{\sigma}_{\mathrm{m}} \rangle_{\Omega_2} = \widehat{\boldsymbol{C}} : \langle \boldsymbol{\sigma}_{\mathrm{m}} \rangle_{\Omega}$ and $\langle \boldsymbol{\sigma}_{\mathrm{m}} \rangle_{\Omega_1} = \widehat{\widehat{\boldsymbol{C}}} : \langle \boldsymbol{\sigma}_{\mathrm{m}} \rangle_{\Omega}$. We remark that the failure stresses, are independent of the applied loads, since they are material parameters. We remark that the relative decrease in $\widehat{\boldsymbol{C}}$ is accompanied by a corresponding increase $\widehat{\widehat{\boldsymbol{C}}}$, since

$$\frac{(\boldsymbol{I} - v_2 \widehat{\boldsymbol{C}})}{1 - v_2} = \widehat{\widehat{\boldsymbol{C}}}. \tag{4.9}$$

In other words, $\frac{\partial \widehat{\widehat{\boldsymbol{C}}}}{\partial \boldsymbol{C}}$ is a negative-definite tensor function. These previous relations simply indicate that when there is amplification of the stresses somewhere in the microheterogeneous solid there is also simultaneous shielding (''de-amplification'') somewhere in the solid. For the second phase

$$N_{\mathrm{f2}} = \frac{1}{2}\left(\frac{\| \langle \boldsymbol{\sigma}_a \rangle_{\Omega_2} \|}{\| \langle \boldsymbol{\sigma}_{\mathrm{f2}} \rangle_{\Omega_2} \| - \| \langle \boldsymbol{\sigma}_{\mathrm{m}} \rangle_{\Omega_2} \|} \right)^{1/b_2} = \frac{1}{2}\left(\frac{\| \widehat{\boldsymbol{C}} : \langle \boldsymbol{\sigma}_a \rangle_{\Omega} \|}{\| \langle \boldsymbol{\sigma}_{\mathrm{f2}} \rangle_{\Omega_2} \| - \| \widehat{\boldsymbol{C}} : \langle \boldsymbol{\sigma}_{\mathrm{m}} \rangle_{\Omega} \|} \right)^{1/b_2}, \tag{4.10}$$

which is a monotonically increasing function of $\widehat{\boldsymbol{C}}$. For the first phase,

$$N_{\mathrm{f1}} = \frac{1}{2}\left(\frac{\| \langle \boldsymbol{\sigma}_a \rangle_{\Omega_1} \|}{\| \langle \boldsymbol{\sigma}_{\mathrm{f1}} \rangle_{\Omega_1} \| - \| \langle \boldsymbol{\sigma}_{\mathrm{m}} \rangle_{\Omega_1} \|} \right)^{1/b_1} = \frac{1}{2}\left(\frac{\| \widehat{\widehat{\boldsymbol{C}}} : \langle \boldsymbol{\sigma}_a \rangle_{\Omega} \|}{\| \langle \boldsymbol{\sigma}_{\mathrm{f1}} \rangle_{\Omega_1} \| - \| \widehat{\widehat{\boldsymbol{C}}} : \langle \boldsymbol{\sigma}_{\mathrm{m}} \rangle_{\Omega} \|} \right)^{1/b_1}, \tag{4.11}$$

which is a monotonically decreasing function of $\widehat{\boldsymbol{C}}$. The rates of increase and decrease of the fatigue lives are controlled by the magnitudes of the b's.

5. Nonconvex–nonderivative genetic search

Due to difficulties with objective function nonconvexity and nondifferentiability we employ a certain class of nonderivative search methods, usually termed ''genetic'' algorithms (GA), which stem from the

pioneering work of John Holland and his colleagues starting the late 1960s [31]. For reviews of such methods, the interested reader is referred to Goldberg [27], Davis [6] or Kennedy and Eberhart [38]. A recent overview of the state of the art of the field can be found in a collection of recent articles, edited by Goldberg and Deb [28]. In Zohdi [67,74] a GA was developed by combining the basic ideas used in the GA community. Presently, we build upon this algorithm further. The central idea is that the microscale parameters form a genetic string and a survival of the fittest algorithm is applied to a population of such strings. The overall process is (I) a population (S) of different designs (strings) are generated at random with the design space, represented by a (''genetic'') string of the design (N) parameters, (II) the performance of each design is tested, (III) the designs are ranked from top to bottom according to their performance, (IV) the best designs are mated pairwise producing two offspring, i.e. each best pair exchanges information by taking random convex combinations of the design components of the parents' genetic strings, (V) the worst performing genetic strings are eliminated and new replacement designs (strings) are introduced into the remaining population of best performing genetic strings and (VI) steps (I–V) are then repeated. An implementation of such ideas is as follows:

- *Step 1:* Randomly select a population of N starting genetic strings, $\mathbf{\Lambda}^i$, $(i = 1, \ldots, N)$, where $\mathbf{\Lambda}^i \stackrel{\text{def}}{=} \{\Lambda_1^i, \Lambda_2^i, \Lambda_3^i, \Lambda_4^i, \Lambda_5^i, \Lambda_6^i, \Lambda_7^i, \ldots\} = \{\kappa_2^i, \mu_2^i, v_2^i, \mathrm{AR}^i, s_1^i, s_2^i, s_3^i, \ldots\}$.
- *Step 2:* Compute the fitness of each string, $\Pi(\mathbf{\Lambda}^i)$, $(i = 1, \ldots, N)$.
- *Step 3:* Rank the genetic strings: $\mathbf{\Lambda}^i$, $(i = 1, \ldots, N)$.
- *Step 4:* Mate the nearest pairs and produce two offspring, $(i = 1, \ldots, N)$

$$\boldsymbol{\lambda}^i \stackrel{\text{def}}{=} \Phi^{(\mathrm{I})}\mathbf{\Lambda}^i + (1 - \Phi^{(\mathrm{I})})\mathbf{\Lambda}^{i+1} \tag{5.1}$$

and

$$\boldsymbol{\lambda}^{i+1} \stackrel{\text{def}}{=} \Phi^{(\mathrm{II})}\mathbf{\Lambda}^i + (1 - \Phi^{(\mathrm{II})})\mathbf{\Lambda}^{i+1}, \tag{5.2}$$

where $0 \leqslant \Phi^{(\mathrm{I})}, \Phi^{(\mathrm{II})} \leqslant 1$, with $\Phi^{(\mathrm{I})}$ and $\Phi^{(\mathrm{II})}$ being different random values for each component.
- *Step 5:* Kill off the bottom $M < N$ strings and keep the top $K < N$ parents (K offspring $+ K$ parents $+ M = N$).
- *Step 6:* Repeat Steps 1–6 with the top gene pool (K offspring and K parents), plus M new, randomly generated, genetic strings.

Remark I: Previous numerical studies by the author, Zohdi [67,74], have found that the retention of the top old fit genetic strings is critical. For sufficiently large populations, the benefits of parent retention outweigh any disadvantages of ''inbreeding'', i.e. a stagnant population, provided sufficient new genes are introduced after each generation. For more details on this so-called ''inheritance property'' see [6,54] or [38]. This stems from the fact that the objective functions are highly nonconvex and there exists a strong possibility that the inferior offspring will replace superior parents. Retaining the top parents is not only less computationally expensive, since these designs do not have to be reevaluated in future generations, it is theoretically superior. [2] With parent retention, the minimization of the cost function is guaranteed to be monotone with increasing generations [74].

Remark II: The overall genetic minimization strategy can be enhanced several ways. For example, every few generations, the search domain can be restricted and rescaled to be centered around the best current design.

[2] The monotonicity is obvious since the top design will not be replaced until a better design is found.

Remark III: Typically, for samples with a finite number of particles, there will be slight variations in the performance for different random realizations. In order to stabilize the objective function's value with respect to the randomness of the realization, for a fixed design ($\mathbf{\Lambda}^I$), a regularization procedure is applied, whereby the performances of a series of different random realizations are averaged until the (ensemble) average converges, i.e. until the following condition is met ($i = 1, 2, \ldots, E$):

$$\left| \frac{1}{E+1} \sum_{i=1}^{E+1} \Pi^{(i)}(\mathbf{\Lambda}^I) - \frac{1}{E} \sum_{i=1}^{E} \Pi^{(i)}(\mathbf{\Lambda}^I) \right| \leqslant \mathrm{TOL} \left| \frac{1}{E+1} \sum_{i=1}^{E+1} \Pi^{(i)}(\mathbf{\Lambda}^I) \right|. \tag{5.3}$$

The index i indicates a random realization that has been generated and E indicates the total number of realizations tested. In order to implement this in Step 2 of the algorithm, one simply replaces "Compute" with "Ensemble-compute", which requires a further inner loop to test the performance of multiple realizations. Similar ideas have been applied to randomly dispersed particulate solids in Zohdi [67]. The number needed to stabilize the objective function is far less than that needed to stabilize the gradients, and higher order derivatives that would be needed *if a gradient-type approach were even possible*.

6. Numerical examples

Throughout the numerical examples, we considered the following objective function:

$$\Pi^P = w_\kappa \underbrace{\left(\frac{\kappa^* - \kappa^{*,\mathrm{D}}}{\kappa^{*,\mathrm{D}}} \right)^2}_{\text{Macrobulk}} + w_\mu \underbrace{\left(\frac{\mu^* - \mu^{*,\mathrm{D}}}{\mu^{*,\mathrm{D}}} \right)^2}_{\text{Macroshear}} + \underbrace{\sum_{q=1}^{10} w_q P_q(\Lambda)}_{\text{Microdistortion}} + \underbrace{w_{\mathrm{F}} P_{\mathrm{F}}}_{\text{Microfatigue}} . \tag{6.1}$$

A meaningful measure to track during the minimization process is the percentage error of the moduli from the desired target, $\sqrt{\Pi^P}$. To illustrate the algorithm, we considered a cube of matrix material, with normalized dimensions $1 \times 1 \times 1$, containing randomly distributed inhomogeneities. We considered the following boundary conditions on the exterior of the cube: $\boldsymbol{u}|_{\partial\Omega} = \bar{\varepsilon} \cdot \boldsymbol{x}$, $\bar{\varepsilon}_{ij} = 0.001$, $i, j = 1, 2, 3$, where $\boldsymbol{x}$ is a position vector to the boundary of the cube. During the upcoming numerical experiments we tested larger and larger samples of material, keeping the volume fraction fixed and found that results stabilized when approximately 20 (nonintersecting) particles were used in a sample, i.e. the same final designs occurred using larger samples. Also, over the course of such tests the finite element meshes were repeatedly refined, and a mesh density of approximately $9 \times 9 \times 9$ trilinear hexahedra (approximately between 2200 and 3000 DOF for the vector-valued balance of momentum) *per particle* was found to deliver mesh independent results. For 20 particles, this resulted in 46,875 DOF. This mesh density delivered mesh independent results over the course of the numerical experiments. In other words, the same final designs occurred using finer meshes. During the computations, a "2/5" Gauss rule was used, whereby elements containing material discontinuities had increased Gauss rules ($5 \times 5 \times 5$) to enhance the resolution of the internal geometry, while elements with no material discontinuities had the nominal $2 \times 2 \times 2$ rule. For details of such meshing procedures, see [67,69–72]. To illustrate the search process, continuing with 20 particle samples, the effective response produced by a sample containing a particulate stiffener, 22% boron ($\mu_1 = 230$ GPa $\kappa_1 = 172$ GPa) spheres in an aluminum matrix ($\mu_1 = 25.9$ GPa $\kappa_1 = 77.9$ GPa) was first computed. [3] The effective response was approximately $\kappa^* = 96$ GPa and $\mu^* = 42$ GPa. Our objective was to find alternative microstructures which could deliver the same effective response ($\kappa^{*\mathrm{D}} = 96$ GPa and $\mu^{*\mathrm{D}} = 42$ GPa), while obeying the

[3] Material combinations such as aluminum/boron are relatively common due to the ease of forming the aluminum matrix and the lightweight of the boron.

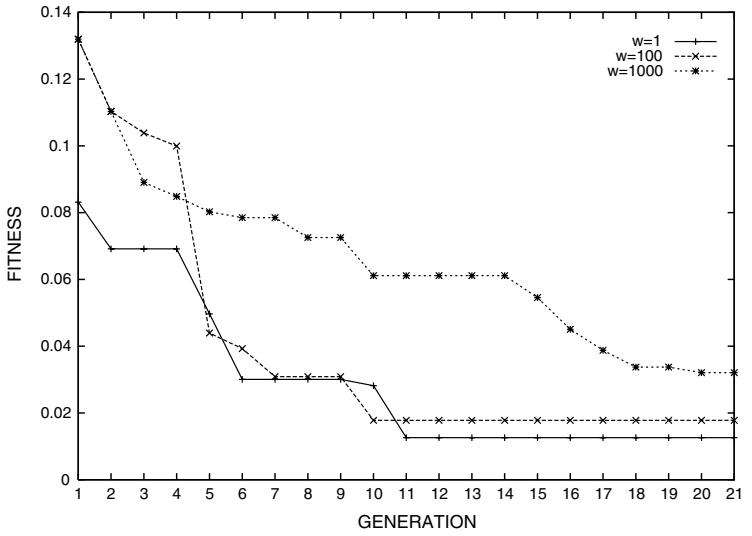

Fig. 3. The top design behavior for various weights after 21 generations. Here fitness $\stackrel{\text{def}}{=} \sqrt{\Pi^P}$. After every four generations the search domain was restricted and rescaled to be centered around the best current design.

constraints, to a specified tolerance. The constraint tolerance for fatigue was $\text{TOL}_\alpha = 0.9$ (10% damage) and for the distortion constraints, $\text{TOL}_q = 0.1, \forall q$. The matrix material was fixed to be aluminum, however, all other design parameters, with the exception of the particle orientations, since isotropic objectives were sought, were allowed to vary. The macroscopic weights were fixed at $w_\kappa = w_\mu = 1$, while the penalty weights were increased. The volume fraction wascontrolled via a particle/sample size ratio (one variable), defined by a subvolume size $V \stackrel{\text{def}}{=} \frac{L\times L\times L}{N}$, where N is the number of particles in the entire sample and where L is the length of the (cubical) sample, $L \times L \times L$. A generalized diameter is defined, r, which is the diameter of the smallest sphere that can enclose a single particle of possibly nonspherical shape. The ratio between the generalized diameter and the subvolume is one design parameter defined by $\zeta \stackrel{\text{def}}{=} \frac{r}{V^{1/3}}$. The a priori constraints on the design search space were

$$\boxed{\begin{aligned}
&0.1\kappa_1 = \kappa_2^- \leqslant \kappa_2^{(i)} \leqslant \kappa_2^+ = 10\kappa_1,\\
&0.1\mu_1 = \mu_2^- \leqslant \mu_2^{(i)} \leqslant \mu_2^+ = 10\mu_1,\\
&0.1 = \text{AR}^- \leqslant \text{AR}^{(i)} \leqslant \text{AR}^+ = 10,\\
&1 = s^- \leqslant s^{(i)} \leqslant s^+ = 10,\\
&0.2 = \zeta^- \leqslant \zeta^{(i)} \leqslant \zeta^+ = 0.4.
\end{aligned}} \tag{6.2}$$

For the fatigue constraints, we characterized the maximum and minimum applied boundary loading in the form [4] $\boldsymbol{u}^{\max}|_{\partial\Omega} = \mathscr{E}_{\max} \cdot \boldsymbol{x} = a^+ \mathscr{E}_{ij}$, and $\boldsymbol{u}^{\min}|_{\partial\Omega} = \mathscr{E}_{\min} \cdot \boldsymbol{x} = a^- \mathscr{E}_{ij}$, $i, j = 1, 2, 3$. For purposes of numerical experiment, the cyclic loading amplitudes were set to $a^- = 0.9$ and $a^+ = 1.25$. The Basquin exponents were chosen to be the same for both materials, $b_1 = -0.06$ and $b_2 = -0.06$, in order to isolate the effects of the seven micromechanical variables introduced earlier on the fatigue behavior. The number of applied cycles

[4] By superposition, one only needs to compute one loading.

was set to $n = 10^5$. The failure stresses for the particles, $\boldsymbol{\sigma}_{f2}$, were set to $\sigma_{f2,ij} = 1$ GPa, $i, j, = 1, 2, 3$, while for the matrix $\boldsymbol{\sigma}_{f1}$, we selected $\sigma_{f1,11} = \sigma_{f1,22} = \sigma_{f1,33} = 8 \times 10^7$ and $\sigma_{f1,12} = \sigma_{f1,23} = \sigma_{f1,31} = 4 \times 10^7$.

The number of genetic strings was set to 20, keeping the offspring of the top six parents after each generation. This resulted in eight new strings being introduced after each generation. After every four generations the search domain was restricted and rescaled to be centered around the best current design. For various penalty weights, the procedure converged to a stable best design in no more than 21 generations (Fig. 3). The total number of global evaluations was $T + (G - 1) \times (T - Q) = 300$, where $G = 21$ was the number of generations, $T = 20$ was the total number of genetic strings in the population, and $Q = 6$ is the number of parents kept after each generation. As the theory predicted (Box (3.6)), at the converged state

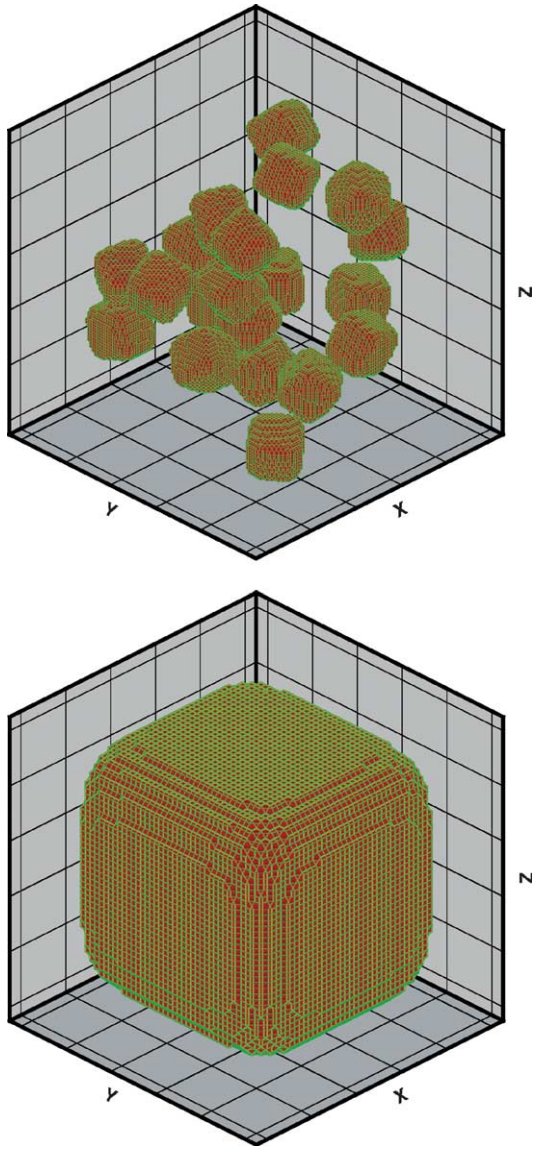

Fig. 4. Top: a realization of the optimal design. Bottom: a zoom on an individual particle.

Table 1
Top design after 21 generations

Penalty	$\sqrt{\Pi^P}$	κ^* (GPa)	μ^* (GPa)	$\langle\alpha\rangle_\Omega$
$w_q = w_F = 1$	0.01260	93.464	40.290	0.92155
$w_q = w_F = 100$	0.01780	92.498	37.716	0.92121
$w_q = w_F = 1000$	0.03208	94.195	38.728	0.90430

Note: $\langle\alpha\rangle_\Omega = 1$ means no estimated damage due to fatigue.

Table 2
Top design after 21 generations

Penalty	κ_2/κ_1	μ_2/μ_1	ζ	v_2	AR	s_1	s_2	s_3	$\sqrt{\Pi^P}$
$w_q = w_F = 1$	4.9755	6.0648	0.22680	0.07524	0.9392	4.9036	5.3449	5.7754	0.01260
$w_q = w_F = 100$	4.1183	6.0271	0.23042	0.07898	1.0065	5.7951	5.0898	3.0565	0.01780
$w_q = w_F = 1000$	5.2445	4.9966	0.23714	0.08668	0.9513	5.6470	6.9010	3.7959	0.03208

Table 3
The number of samples needed for ensemble average stabilization for various penalty weights

Penalty	Total samples	Total samples/genetic string
$w_q = w_F = 1$	5616	18.720
$w_q = w_F = 100$	5251	17.503
$w_q = w_F = 1000$	4837	16.123

(generation 21), with increasing penalty weights $\Pi^P(\mathbf{\Lambda}_K^*, \boldsymbol{w}^K)$ converges from below. There were no changes in the results for further increases in the penalty weights beyond $w_q = w_F = 1000$. Clearly, the constraints restrict the objective from ever attaining the original spherical microstructure, and thus effective properties, $\kappa^* = 96$ GPa and $\mu^* = 42$ GPa, that deliver a zero value of the unconstrained objective function (Fig. 4). Various statistics pertaining to these test are tabulated in Tables 1–3.

7. Concluding remarks

In this work a GA was developed which can handle difficulties due to objective function nonconvexity and lack of regularity characterizing the constrained design of random particulate media. The computational approach was constructed in such a way that it can be used in conjunction with a variety of methods designed for large-scale micro–macro simulations, such as *multiscale methods* [2,4,8–18,64]; *Voronoi cell methods* [20–26,43,44,49,56]; *transformation methods* [46,50], *multipole methods* adapted to such problems by Fu et al. [19]; *partitioning methods* [29,30,32–37]; *adaptive hierarchical modeling methods* [48,51–53,63,65] and *micro–macro domain decomposition* [3,39–42,66,69–71,73].

References

[1] O.H. Basquin, The exponential law of endurance tests, Proc. Am. Soc. Testing Mater. 10 (1910) 625–630.
[2] V. Belsky, M.W. Beall, J. Fish, M.S. Shephard, S. Gomaa, Computer-aided multiscale modeling tools for composite materials and structures, Int. J. Comput. Syst. Engrg. 6 (3) (1995) 213–223.
[3] L. Champaney, J. Cognard, D. Dureisseix, P. Ladeveze, Large scale applications on parallel computers of a mixed domain decomposition method, Comput. Mech. 19 (4) (1997) 253–263.

[4] W. Chen, J. Fish, A dispersive model for wave propagation in periodic heterogeneous media based on homogenization with multiple spatial and temporal scales, J. Appl. Mech. 68 (2) (2001) 153–161.
[5] A. Cherkaev, Variational Methods for Structural Optimization, Springer-Verlag, 2000.
[6] L. Davis, Handbook of Genetic Algorithms, Thompson Computer Press, 1991.
[7] A.V. Fiacco, G.P. McCormick, Nonlinear Programming: Sequential Unconstrained Minimization Techniques. Siam reissue, John Wiley and Sons, New York and Toronto, 1990.
[8] J. Fish, A. Wagiman, Multiscale finite element method for a locally nonperiodic heterogeneous medium, Comput. Mech. 12 (1993) 164–180.
[9] J. Fish, M. Pandheeradi, V. Belsky, An efficient multilevel solution scheme for large scale nonlinear systems, Int. J. Numer. Meth. Engrg. 38 (1995) 1597–1610.
[10] J. Fish, V. Belsky, Multigrid method for periodic heterogeneous media Part I: convergence studies for one dimensional case, Comput. Methods Appl. Mech. Engrg. 126 (1995) 1–16.
[11] J. Fish, V. Belsky, Multigrid method for periodic heterogeneous media Part II: multiscale modeling and quality control in multidimensional case, Comput. Methods Appl. Mech. Engrg. 126 (1995) 17–38.
[12] J. Fish, V. Belsky, Generalized aggregation multilevel solver, Int. J. Numer. Meth. Engrg. 40 (1997) 4341–4361.
[13] J. Fish, K. Shek, M. Pandheeradi, M.S. Shephard, Computational plasticity for composite structures based on mathematical homogenization: theory and practice, Comput. Methods Appl. Mech. Engrg. 148 (1–2) (1997) 53–73.
[14] J. Fish, Q. Yu, K.L. Shek, Computational damage mechanics for composite materials based on mathematical homogenization, Int. J. Numer. Meth. Engrg. 45 (1999) 1657–1679.
[15] J. Fish, K. Shek, Finite deformation plasticity for composite structures: computational models and adaptive strategies, Comput. Methods Appl. Mech. Engrg. 172 (1999) 145–174.
[16] J. Fish, A. Ghouli, Multiscale analytical sensitivity analysis for composite materials, Int. J. Numer. Meth. Engrg. 50 (2001) 1501–1520.
[17] J. Fish, Q. Yu, Multiscale damage modeling for composite materials: theory and computational framework, Int. J. Numer. Meth. Engrg. 52 (1–2) (2001) 161–192.
[18] J. Fish, W. Chen, Uniformly valid multiple spatial–temporal scale modeling for wave propagation in heterogeneous media, Mech. Compos. Mater. Struct. 8 (2001) 81–99.
[19] Y. Fu, K. Klimkowski, G.J. Rodin, E. Berger, J.C. Browne, J.K. Singer, R.A. Van de Geijn, K. Vemaganti, Fast solution method for three-dimensional many-particle problems of linear elasticity, Int. J. Numer. Meth. Engrg. 42 (1998) 1215–1229.
[20] S. Ghosh, S.N. Mukhopadhyay, A material based finite element analysis of heterogeneous media involving Dirichlet tessellations, Comput. Methods Appl. Mech. Engrg. 104 (1993) 211–247.
[21] S. Ghosh, S. Moorthy, Elastic–plastic analysis of arbitrary heterogeneous materials with the Voronoi cell finite element method, Comput. Methods Appl. Mech. Engrg. 12 (1–4) (1995) 373–409.
[22] S. Ghosh, L. Kyunghoon, S. Moorthy, Two scale analysis of heterogeneous elastic–plastic materials with asymptotic homogenization and Voronoi cell finite element model, Comput. Methods Appl. Mech. Engrg. 132 (1–2) (1996) 63–116.
[23] S. Ghosh, S. Moorthy, Particle fracture simulation in non-uniform microstructures of metal–matrix composites, Acta Mater. 46 (3) (1998) 965–982.
[24] S. Ghosh, K. Lee, P. Raghavan, A multi-level computational model for multi-scale damage analysis in composite and porous materials, Int. J. Solids Struct. 38 (2001) 2335–2385.
[25] S. Ghosh, Y. Ling, B. Majumdar, R. Kim, Interfacial debonding analysis in multiple fiber reinforced composites, Mech. Mater. 32 (2001) 562–591.
[26] S. Ghosh, L. Kyunghoon, S. Moorthy, Two scale analysis of heterogeneous elastic–plastic materials with asymptotic homogenization and Voronoi cell finite element model, Comput. Methods Appl. Mech. Engrg. 132 (1–2) (1996) 63–116.
[27] D.E. Goldberg, Genetic Algorithms in Search, Optimization and Machine Learning, Addison-Wesley, 1989.
[28] D.E. Goldberg, K. Deb, Special issue on genetic algorithms, Comput. Methods Appl. Mech. Engrg. 186 (2–4) (2000) 121–124.
[29] S. Hazanov, C. Huet, Order relationships for boundary conditions effect in heterogeneous bodies smaller than the representative volume, J. Mech. Phys. Solids 42 (1994) 1995–2011.
[30] S. Hazanov, M. Amieur, On overall properties of elastic heterogeneous bodies smaller than the representative volume, Int. J. Engrg. Sci. 33 (9) (1995) 1289–1301.
[31] J.H. Holland, Adaptation in Natural and Artificial Systems, University of Michigan Press, Ann Arbor, Michigan, 1975.
[32] C. Huet, Universal conditions for assimilation of a heterogeneous material to an effective medium, Mech. Res. Commun. 9 (3) (1982) 165–170.
[33] C. Huet, On the definition and experimental determination of effective constitutive equations for heterogeneous materials, Mech. Res. Commun. 11 (3) (1984) 195–200.
[34] C. Huet, Application of variational concepts to size effects in elastic heterogeneous bodies, J. Mech. Phys. Solids 38 (1990) 813–841.

[35] C. Huet, Hierarchies and bounds for size effects in heterogeneous bodies, in: G.A. Maugin (Ed.), Continuum Models and Discrete Systems, vol. 2, 1991, pp. 127–134.
[36] C. Huet, An integrated micromechanics and statistical continuum thermodynamics approach for studying the fracture behaviour of microcracked heterogeneous materials with delayed response, Engrg. Fract. Mech. 58 (5–6) (1997) 459–556, special issue.
[37] C. Huet, Coupled size and boundary condition effects in viscoelastic heterogeneous bodies, Mech. Mater. 31 (12) (1999) 787–829.
[38] J. Kennedy, R. Eberhart, Swarm Intelligence, Morgan Kaufmann Publishers, 2001.
[39] P. Ladeveze, O. Loiseau, D. Dureisseix, A micro–macro and parallel computational strategy for highly heterogeneous structures, Int. J. Numer. Meth. Engrg. 52 (1/2) (2001) 121–138.
[40] P. Ladeveze, D. Dureisseix, A micro/macro approach for parallel computing of heterogeneous structures, Int. J. Comput. Civil Struct. Engrg. 1 (1) (2000) 18–28.
[41] P. Ladeveze, D. Dureisseix, Une nouvelle stratégie de calcul micro/macro en mécanique des strutures, CRAS Série IIB 327 (1999) 1237–1244.
[42] P. Ladeveze, A modelling error estimator for dynamic structural model updating, in: P. Ladeveze, J.T. Oden (Eds.), Advances in Adaptive Computational Methods in Mechanics (Proc. of the Workshop on New Advances in Adaptive Computational Methods in Mechanics, Cachan, 1997), Elsevier, 1998, pp. 135–151.
[43] K. Lee, S. Moorthy, S. Ghosh, Multiple scale computational model for damage in composite materials, Effective properties of composite materials with periodic microstructure: a computational approach, Comput. Methods Appl. Mech. Engrg. 172 (1999) 175–201.
[44] M. Li, S. Ghosh, O. Richmond, An experimental–computational approach to the investigation of damage evolution in discontinuously reinforced aluminum matrix composite, Acta Mater. 47 (12) (1999) 3515–3532.
[45] D. Luenberger, Introduction to Linear and Nonlinear Programming, Addison-Wesley, Menlo Park, 1974.
[46] J.C. Michel, H. Moulinec, P. Suquet, Effective properties of composite materials with periodic microstructure: a computational approach, Comput. Methods Appl. Mech. Engrg. 172 (1999) 109–143.
[47] M.A. Miner, Cumulative damage in fatigue, J. Appl. Mech. 12 (1945) 159–164.
[48] N. Moes, J.T. Oden, T.I. Zohdi, Investigation of the interaction of numerical error and modeling error in the homogenized Dirichlet projection method, Comput. Methods Appl. Mech. Engrg. 159 (1998) 79–101.
[49] S. Moorthy, S. Ghosh, Adaptivity and convergence in the Voronoi cell finite element model for analyzing heterogeneous materials, Comput. Methods Appl. Mech. Engrg. 185 (2000) 37–74.
[50] H. Moulinec, P. Suquet, A numerical method for computing the overall response of nonlinear composites with complex microstructure, Comput. Methods Appl. Mech. Engrg. 157 (1998) 69–94.
[51] J.T. Oden, T.I. Zohdi, Analysis and adaptive modeling of highly heterogeneous elastic structures, Comput. Methods Appl. Mech. Engrg. 148 (1997) 367–391.
[52] J.T. Oden, K. Vemaganti, Adaptive hierarchical modeling of heterogeneous structures, Physica D 133 (1999) 404–415.
[53] J.T. Oden, K. Vemaganti, N. Moes, Hierarchical modeling of heterogeneous solids, Comput. Methods Appl. Mech. Engrg. 172 (1999) 1–27.
[54] C. Onwubiko, Introduction to Engineering Design Optimization, Prentice Hall, 2000.
[55] A. Palmgren, Die Lebensdauer von kugellagern, Z. Vereins Deut. Ingenieure 68 (1924) 339–341.
[56] P. Raghavan, S. Moorthy, S. Ghosh, N.J. Pagano, Revisiting the composite laminate problem with an adaptive multi-level computational model, Compos. Sci. Technol. 61 (2001) 1017–1040.
[57] S. Suresh, Fatigue of Materials, second ed., Cambridge University Press, 1998.
[58] S. Torquato, Random heterogeneous media: microstructure and improved bounds on effective properties, Appl. Mech. Rev. 44 (1991) 37–76.
[59] S. Torquato, Effective stiffness tensor of composite media I. Exact series expansions, J. Mech. Phys. Solids 45 (1997) 1421–1448.
[60] S. Torquato, Effective stiffness tensor of composite media II. Applications to isotropic dispersions, J. Mech. Phys. Solids 46 (1998) 1411–1440.
[61] S. Torquato, Random Heterogeneous Materials: Microstructure and Macroscopic Properties, Springer-Verlag, New York, 2002.
[62] S. Torquato, S. Hyun, Effective-medium approximation for composite media: realizable single-scale dispersions, J. Appl. Phys. 89 (2001) 1725–1729.
[63] K.S. Vemaganti, J.T. Oden, Estimation of local modeling error and goal-oriented adaptive modeling of heterogeneous materials, Comput. Methods Appl. Mech. Engrg. 190 (2001) 46–47, 6089–6124.
[64] R. Wentorf, R. Collar, M.S. Shephard, J. Fish, Automated modeling for complex woven mesostructures, Comput. Methods Appl. Mech. Engrg. 172 (1999) 273–291.
[65] T.I. Zohdi, J.T. Oden, G.J. Rodin, Hierarchical modeling of heterogeneous bodies, Comput. Methods Appl. Mech. Engrg. 138 (1996) 273–298.
[66] T.I. Zohdi, P. Wriggers, A domain decomposition method for bodies with microstructure based upon material regularization, Int. J. Solids Struct. 36 (17) (1999) 2507–2526.
[67] T.I. Zohdi, On the tailoring of microstructures for prescribed effective properties, Int. J. Fract. 114 (2002) L15–L20.

[68] T.I. Zohdi, Bounding envelopes in multiphase material design, J. Elasticity 66 (2002) 47–62.
[69] T.I. Zohdi, P. Wriggers, Aspects of the computational testing of the mechanical properties of microheterogeneous material samples, Int. J. Numer. Meth. Engrg. 50 (2001) 2573–2599.
[70] T.I. Zohdi, P. Wriggers, Computational micro-macro material testing, Arch. Comput. Meth. Engrg. 8 (2) (2001) 131–228.
[71] T.I. Zohdi, P. Wriggers, C. Huet, A method of substructuring large-scale computational micromechanical problems, Comput. Methods Appl. Mech. Engrg. 190 (2001) 43–44, 5639–5656.
[72] T.I. Zohdi, Computational optimization of vortex manufacturing of advanced materials, Comput. Methods Appl. Mech. Engrg. 190 (2001) 46–47, 6231–6256.
[73] T.I. Zohdi, Statistical ensemble error bounds for homogenized microheterogeneous solids, J. Appl. Math. Phys. (Z. Angew. Math. Phys.), in press.
[74] T.I. Zohdi, Genetic optimization of statistically uncertain microheterogeneous solids, Philos. Trans. Roy. Soc. Vol. 361, No. 1806, pp. 1021–1043.